535

Egypt. J. Chem. **Vol. 65,** No. 8, pp. 499 – 509 (2022)

Egyptian Journal of Chemistry

http://ejchem.journals.ekb.eg/

Physical, Optical and Radiation Shielding Properties of Some Phosphate Glasses

M. Hammam,[1] E. Kilany, [1*] E. Nabhan,[2] A. Abdel Moghny, [2] A. Atta, [3,4]

[1] *Department of physics, Faculty of Science, Helwan University.*
[2] *Physics Department, Faculty of Science, Al-Azhar University, Girls' branch.*
[3] *Physics Department, College of Science, Jouf University, P.O. Box: 2014, Sakaka, Saudi Arabia.*
[4] *Radiation Physics Department, National Center for Radiation Research and Technology (NCRRT), Atomic Energy Authority (AEA), Cairo, Egypt.*

Abstract

Glass systems xPbO-(50-x)ZnO-50(P_2O_5) (where x = 0,10,20,30,40,50 mol%) were made using the traditional melt quench method. The produced samples' amorphous phase was confirmed by x-ray diffraction (XRD). The effect of replacing Zn^{2+} with Pb^{2+} ions on the chemical structure of the studied system was investigated using Fourier-transform infrared (FTIR) in the range 400-4000 cm^{-1}. Moreover, the optical constants such as refractive index, absorption coefficient, extinction coefficient, optical band gap, and optical conductivity have been calculated using UV-Visible spectroscopy. Density, Molar volume, and hardness were measured, and they are found to be composition-dependent. ^{60}Co (6.95μci) and ^{137}Cs (10μci) radioactive sources were used to investigate the attenuation of gamma rays through the samples. The basic shielding quantities for determining the penetration of radiation in glass, such as mass attenuation coefficient (μ/ρ) and half value layer (HVL) were investigated experimentally and theoretically. The results proved that the prepared glass samples possess superior gamma-ray shielding effectiveness.
Keywords: Radiation shielding material, Phosphate glass, Energy gap, Optical Absorption, Infrared deconvolution, Hardness.*Keywords:* Type your keywords here, separated by semicolons ;

1. Introduction

As technology advances, a large majority of equipment are reliant on radiation to function effectively. Radiation is defined as "the transmission of energy via a medium or substance".[1] Despite its numerous real hazards, radiation is necessary for advances in health, agricultural production, power production, space research, and several other sectors. To avoid its harmful effects, one of the solutions is shielding with one of the shielding materials that can mitigate the effects of exposure. It has the capability of absorbing rays and reduce the intensity to acceptable levels. Alloys, concretes, and glasses are common shielding rays components. Because of its favorable insulating qualities, including variety in composition, cheap production cost, and excellent attenuation ability, glasses are frequently employed as radiation shields. They also provide the ability to look through. Glasses can also be easily made utilizing a variety of standard processes, such as the "melt quenching method" or the "sol-gel method" [1][2][3].

In this paper, we discuss and study phosphate glass because it is one of the best glass formers and has a lot of competitive characteristics such as: Low melting temperature, low crystallization ability, high stability, high dielectric constant, high thermal stability, low phonon energy, and adequate infrared ray passage over a range of energies. However, its hygroscopic nature and low chemical resistance have restricted its use[5].

There have been several researches carried out to enhance phosphate glass's physical characteristics and chemical endurance, including various metal oxides, such as Pb and Zn, into the network [6][7]. PbO is a metallic oxide that expands the chemical stability of phosphate glass due to the number of factors since (Pb^{2+}) ions improve its chemical stability via formed "P-O-Pb" bonding. PbO enhances the moistness resistance of the formed glass[8].

The incorporated zinc oxide in glass structures is expected to act as an intermediate oxide either as network former or as network modifier. As former, ZnO enters the network with ZnO_4 structural units and as network modifier, zinc ions are octahedrally coordinated and behaves like any other conventional alkali oxides. Besides, adding Zn to the phosphate glass contributes to the conception of "non-bridging oxygen atoms (NBOs)" [9].

Recently, zinc oxide-derived composite significantly drew investigators' attention due to its unique characteristics such as direct wide band gap, being nontoxic material, its non-hygroscopic nature, lower price, intrinsic emitting characteristics, and large exciton binding energy. And according to the previous mentioned characteristics, it is found that Glasses made of "PbO-ZnO-P_2O_5" have improved chemical and physical endurance while keeping low glass conversion and softening points.[8]. Furthermore, the production and classification of ternary "PbO-ZnO-P_2O_5" glasses offer glass-to-metal sealant possibility in nuclear reactor windows, isotope handling facilities, and any other increased irradiation region where dramatic irradiation mitigation is needed [8]. As a result, "PbO-ZnO-P_2O_5-derived" glasses have been proven to be more effective insulating glasses than "PbO-derived glasses".

The primary objective of this research is to investigate the physical, structural, optical, and shielding characteristics of "PbO-ZnO-P_2O_5" glasses as a viable shielding option.

2. Methodology

2.1 Preparation method

Transparent phosphate glasses of nominal composition $xPbO$-$(50-x)ZnO$-$50P_2O_5$ where x from 0 to 50 mol % were prepared by conventional melt quench method. P_2O_5 which was prepared from ammonium dehydrogenate phosphate ($NH_4H_2PO_4$) and Pb ions, was introduced at the main component's expense in increasing percent (0, 10, 20, 30, 40 and 50 mol%) to the base host glass. The six samples were well mixed and weighed and the error was taken in consideration to get accurate weights. Then they were put at 600°C in a previously heated muffle furnace. When the heat reached 650°C, the ammonia and water were evaporated. The furnace was raised gradually till 1000°C for 3 hours to reach complete melting and mixing. Finally, they were poured on a stainless-steel mold to get the desired shape and thickness.

Part of the prepared samples were grinded to be used for different purposes XRD, and IR. Other parts were polished for optical characterization, hardness, and γ-attenuation.

2.2 Characterization techniques

X-ray diffraction measurements were used to settle the surface morphology of the specimens by the aid of "computerized X-ray diffractometer (Shimadzu XRD-6000), NCRRT, Cairo, Egypt, with 2θ range between 4° to 90° and applying a scan rate of 2°/min".

2.3 Molar volume and density

Compactness was estimated by applying the "Archimedes method" and by using immersing toluene as an immersing fluid ($\rho = 0.8669$ gm cm^{-3}). The experimental densities were obtained at ambient conditions. The weight of every glass specimen was measured in air and in toluene three times for each sample, and then the average value was calculated to determine more accurate density. Density was determined by applying the "Archimedes method" according to;[10]

$$\rho = \frac{W_a}{W_a - W_t} \rho_t \tag{1}$$

In which "w_a" and "w_t" is the specimen masses in airborne and toluene, correspondingly. The density of the buoyant is ρ_t. Then, using the relationship, the molar volume was calculated.;[11]

$$V_m = M/\rho \tag{2}$$

Where M stands for molecular mass and ρ stands for glass density.

2.4 FTIR

For analyzing the chemical changes in the samples, "Fourier-transform infrared (FTIR) analysis" of the prepared glasses was achieved utilizing "AT1 Mattson model Genesis Series (USA) infra-red spectrophotometer". The KBr method was applied to all samples under examination, approximating quantitatively because the sample and KBr weights were fixed. The absorption spectrum of Infrared ranges within "400–4000 cm^{-1}" were recorded at ambient temperature.

2.5 Optical properties

Lead Zinc Phosphate glasses were subjected to optical UV–visible absorption within the range "200–1100 nm". The measurements were carried out by an "UV-spectrophotometer model V-570 (JASCO, Japan)" to investigate the constructed glasses' optical characteristics, the good and polished specimen.

2.6 Hardness

The micro-hardness of the specimen was deduced automatically using "Shimadzu Vickers microhardness tester". The specimens were thoroughly polished to get a smooth and flat parallel surface then they opposed to a load of 200 gm for ١٥ sec.

2.7 Gamma attenuation

A "collimated beam of gamma-rays" released from "^{60}Co (6.95μci)" and "^{137}Cs (10μci)", that were utilized as gamma-ray energy sources. Fig. 1 displays a schematic representation of a γ-ray detection system, in which the γ-ray intensities for

the examined energy lines were measured using a 3″ x 3″ NaI(Tl) scintillation detector. The disc-shaped specimens were polished to have parallel sides. The "Beer-Lambert's equation" was used to assess the "coefficient of linear attenuation", based on the γ-ray energies that passed via the specimens under investigation. The half-value layer "HVL" for every specimen content and total γ-rays was then calculated utilizing the formula below[12][13]

$$I = I_o\, e^{-\mu x} \tag{3}$$
$$HVL = ln2 / \mu \tag{4}$$

In which μ is the sample's "linear attenuation coefficient", I_x and I_o are the γ-rays strengths after and before transmitting via the specimen, and x is the specimen's thickness.

The "mass attenuation coefficient is denoted as (σ, cm^2 /g)"; on the contrary, the critical nuclear property that is unrelated of the overall compactness of the material and was evaluated by [14].

$$\sigma = \frac{\mu}{\rho} \tag{5}$$

The outcome obtained "mass attenuation coefficient" was associated with the designed outcomes by "WinXCom computer program (version 3.1)" for every specimen.

Finally, the mean free path is calculated. It is described as "the average traveled distance between two successive photon interactions". The inferior "MFP" implies numerous is γ-ray interactions with the material, resulting in higher γ-ray shielding efficiency[2]. The following formula may be used to determine the "MFP" of the chosen glass systems [15].

$$MFP = 1 / \mu \tag{6}$$

In which μ is the "coefficient of linear attenuation"

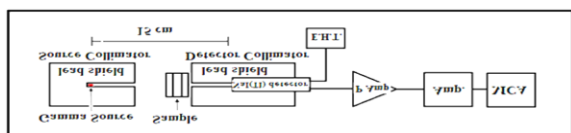**Fig. 1:** Investigational setup for γ-rays spectroscopy shown schematically

3 Results

3.1 Structural characteristics

In X-ray diffraction patterns of the produced samples, no continuous or discrete sharp peaks that indicate the crystalline phase were found; instead, a broad halo was detected, as seen in Fig.2, which indicates the amorphous phase of the obtained substances.

3.2 Density and molar volume

The compactness of glass is measured to assess structural density, interstitial gaps, and coordination number. It is a macroscopic characteristic that increases the density of a

structure by incorporating heavier molecules rather than lightweight ones [16].

Fig.3 shows the experimental density and molar volume. It is detected that density upsurges linearly with the cumulative lead ratio. This is expected since the molecular mass of PbO (223.20) is higher than the molecular mass of ZnO (81.41).

Also, Fig.3 displays that the molar volume rises as density directly with "PbO content". This implies that the free volume of glass increases. Lead's ionic diameters in various coordination states are greater than zinc's. So, replacing a small size atom (Zn) with a large size atom (Pb) increases the glass's free volume, and hence the molar volume [17].
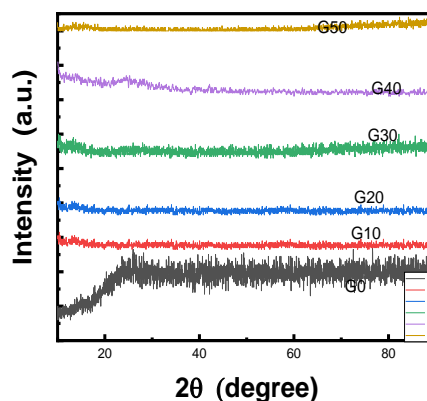

Fig.2: X-ray diffraction patterns of xPbO- (50-x) ZnO-50P$_2$O$_5$ glass "x = 0, 10, 20,30,40 and 50 mol%"
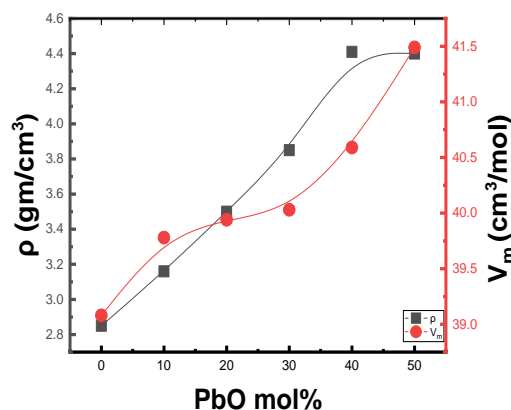

Fig. 3: Variation of the experimental density and molar volume of of xPbO-(50-x) ZnO-50P$_2$O$_5$ where PbO = 0,10,20,30,40 and 50mol %.

3.3 Hardness

The requirement of "Vickers microhardness H$_v$" on the PbO content is shown in Fig.4 and Table1. It's worth noting that as the PbO level rises, so does the glass hardness. It is well known that when the flow mobility of the matrix element decreases, the hardness upsurges. This was backed up by the findings of the viscosity investigations [14]. He proposed that reducing the current pathway in a glass containing oxides is responsible for the rise in

the hardness number of various oxides. The molar volume findings show that Pb has a greater ionic radius than Zn. The substituting of Zn with Pb reduces flow mobility and increases hardness so the investigated glass sample with 50 mol% PbO has the highest value of hardness [10]
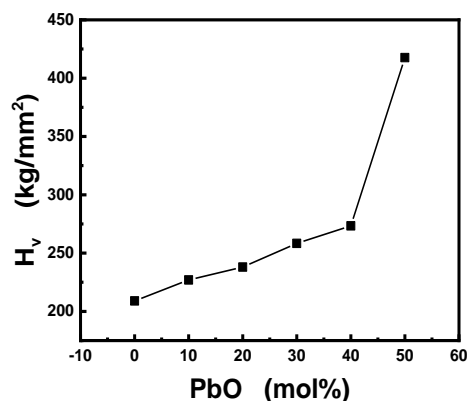

Fig. 4. Microhardness of xPbO-(50-x)ZnO-50P$_2$O$_5$ where PbO = 0,10,20,30,40 and 50mol %.

Table1: The values of Hardness for the samples at all concentration of PbO.

Sample	Hardness(kg/mm^2)
0PbO	219.33
10PbO	227.00
20PbO	238.00
30PbO	258.33
40PbO	273.33
50PbO	417.66

3.4 FTIR

The "IR vibrational bands" are structural fingerprints that are equivalent to similar units in crystalline counterparts [18]. The chemical characterization, especially the ratio of the constitutional network producing oxide, is predicted to affect the "IR vibrational bands".

Adding a modifier oxide to the phosphate network leads to a gradual change in its structural units from Q^3 to Q^2 to depolymerized Q^1/Q^0 glasses. So, the addition ratio of oxide to phosphate determines its type.
In our study, the ratio of phosphate is constant and equals 50 mol% so its type is metaphosphate. In metaphosphate configurations, some PbO arrives the tetrahedral locations to produce PbO$_4$ pyramid (glass former) while all the Pb^{2+} ions and residual Zn^{2+} ions dominate the controlling location among chains [17].

The "FTIR spectra" of the investigated glass "ZnO-P$_2$O$_5$-PbO" ranging from "400-2000 cm^{-1}" as shown in Fig. 5 which reveals the phosphates' typical

absorption bands, as well as a minor absorption band at "~1600 cm^{-1}" credited to "the bending vibrations of O-H bonds" fetched throughout the formation of the KBR pellets by moisture in the air for "FTIR" measures[19]. Consequently, the functional spectral domain for the changes of the structure concerns ranging from "400-1600 cm^{-1}". Five absorption bands were visible in the "FTIR spectra's" main characteristics at ~1266, ~1083, ~908, ~738 and ~538 cm^{-1}.

Examination of the spectra in Fig.5 demonstrates that these spectra are almost identical, with the exception of a minor shift in band locations and occasionally variations in the relative intensities of the major bands.
According to evidence gathered from prior research [17], [10] [20] the following assignments can be understood as follows:

–   The peaks ranged between (1631-1645) cm^{-1} are connected to vibrations of OH, water, POH.
–   The solid and sharp IR band near "1230–1266 cm^{-1}", is attributed to asymmetric stretching modes of the two NBOs bonded to phosphorus atoms, (PO$_2$)$_{as}$ or Q^2 units, in the phosphate tetrahedra)[21]
–   The absorption peaks located between "1013 and 1120 cm^{-1}" were assigned to the asymmetric stretching vibration of P–O mode.
–   However, as shown in fig.5 there is a kink of small intensity ranging from "1043" to "1109 cm^{-1}" distinguished by deconvolution of the spectra into their individual peaks. This kink can be reportedly as a sign of the existence of P–O–Pb (Zn) [22] [17]
-   The absorption band, which is located at "1047-1083 cm^{-1}" was denoted to P-O$^-$.
–   The absorption bands at "893–909 cm^{-1}" and at "713 and 738 cm^{-1}" were denoted to the asymmetric stretching vibration of P–O–P mode and to the symmetric stretching of P–O–P groups, respectively.
–   The bands that ranged between "481–538 cm^{-1}" can be denoted as an O-P-O bending group. It is observed that the band between "544–604 cm^{-1}" strongly appears at G0 since there is no lead so this band can be considered as an indication for Zn–O tetrahedral bonds. Such suggested attributions of the observed bands in the IR spectra are summarized in table 2.

Fig. 6 shows an example of the deconvoluted spectra for G20 sample, and the results are given in table 2. To learn more about the key measurements, a deconvolution procedure should be used.
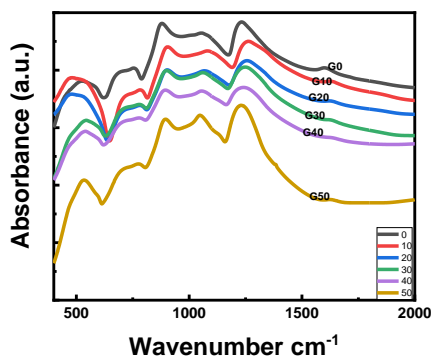
Fig.5: The IR spectra of xPbO- (50-x)ZnO-50P$_2$O$_5$ glass system. G0, G10, G20, G30, G40 and G50 for PbO = 0,10,20,30,40 and 50mol % respectively.
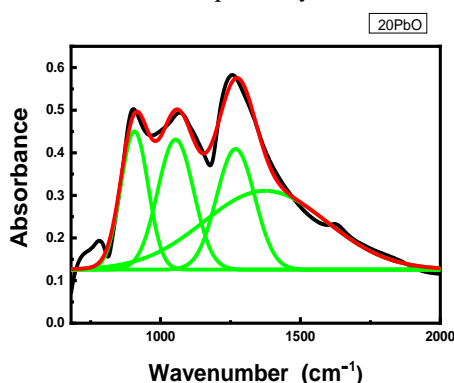

Fig. 6: Band deconvolution of "IR spectrum" for glass sample G20. The red line indicates the The "IR spectra"

Table2: XC is the centre of the band (cm^{-1}) and RA is the relative area (%) of the component band

	G0	G10	G20	G30	G40	G50
XC1	561.7321	496.646	494.5515	549.3239	543.2731	537.8797
RA1	0.01944	0.0724	0.07328	0.02059	0.02457	0.02388
XC2	753.8118	764.1224	762.5483	728.6277	738.9773	724.4258
RA2	0.05334	0.01361	0.01445	0.08923	0.05969	0.06465
XC3	906.2762	902.0412	898.853	936.9728	884.6715	886.9513
RA3	0.10137	0.10827	0.10728	0.14762	0.02164	0.0261
XC4	1055.082	1060.601	1054.5	888.9584	1039.708	1075.511
RA4	0.29827	0.32111	0.33023	0.32764	0.29649	0.32834
XC5	1262.123	1256.247	1247.835	1077.677	1268.174	931.6309
RA5	0.04791	0.04459	0.06882	0.02132	0.08288	0.17138

By analysis of the deconvoluted spectra it was found that:

- Fig. 7 shows that the relative area of P-O$^-$ increased as PbO replaces the ZnO, and this may be due to the increase of NBOs. Since the large

  volume of lead break bonds and create NBOs. Also, the relative area of O-P-O increased as the ratio of PbO increased because of the formation of P-O-Pb.

- In Fig. 8 the position of the bands at ~908, ~753, ~561 cm^{-1} which is belonged to P-O-P$_{asy}$, P-O-P$_{sy}$, PO$_4$ bending, respectively, have changed slightly to a higher wavenumber. However, the

band's position of ~1266 and 1083 cm^{-1}, which correspond to O-P-O and P-O$^-$ have been shifted towards lower wavenumber as the ratio of PbO increases obviously compared to the others. The involvement of Pb^{2+} cations interacting mess of phosphate chains across Q^2 tetrahedra might explain this. Chahine et al., expected that because phosphate chains have a more vital interaction with Pb^{2+} than Zn^{+2} because of the increased electronegativity of the lead ions (1.88) than that of the zinc ions (1.65), thus the phosphorus-oxygen bonds linked to lead ions in P---O-(Pb) would be more substantial than the bonds in P-O---(Zn) and the observed band was moved to a lower wavenumber as a result of this.
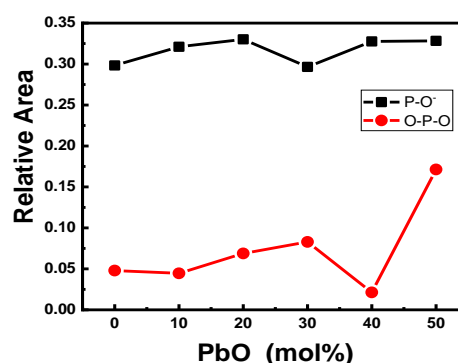

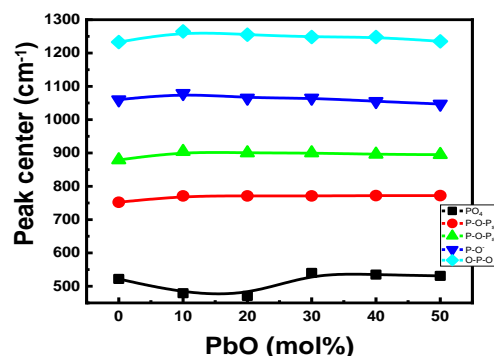**Fig. 7.** Relative area of P-O$^-$ and O-P-O with the concentration of lead.

Fig. 8. Peak center of PO$_4$, P-O-P$_{sy}$, P-O-P$_{asy}$, P-O$^-$ and O-P-O with the concentration of Pb.

3.5 Optical Spectra

The spectrum distribution of the "refractive index *(n)*", the "extinction coefficient *(k)*", and hence the "absorption coefficient *(α)*" is investigated using optical characteristics.

In this section, we study the transmittance and reflectance for studied samples. The obtained data are analyzed to obtain the optical constants *(n)*, *(k)* and *(α)*. The optical band gap E$_g$, the band tail width, and the type of the transitional mechanisms involved were determined by a study of the absorption coefficient.

3.5.1 Curves of refractive index and extinction

coefficient dispersion

The ultraviolet (UV)-visible transmission *(T)* and reflectance *(R)* spectra of the prepared glass samples are shown in Fig.9(a, b). These spectral distribution curves have been used to compute the refractive index, *(n)*, according to the following equation [23]

$$R = \frac{(n+1)^2 + k^2}{(n-1)^2 + k^2} \qquad (7)$$

When k is less than n then we use;

$$n = \frac{1 + \sqrt{R}}{1 - \sqrt{R}} \qquad (8)$$

While the "absorption coefficient (α)" for the studied samples was estimated by the aid of [23]

$$\alpha = \frac{1}{x} \frac{(1-R)^2}{T} \qquad (9)$$

where x is the thickness of the sample, and so the extension coefficient can be obtained by [24].

$$K = \frac{\alpha \lambda}{4\pi} \qquad (10)$$

Fig.10 (a, b) show the "refractive index (n)", and the "extension coefficient (k)" as a "function of wavelength (λ)" [23]
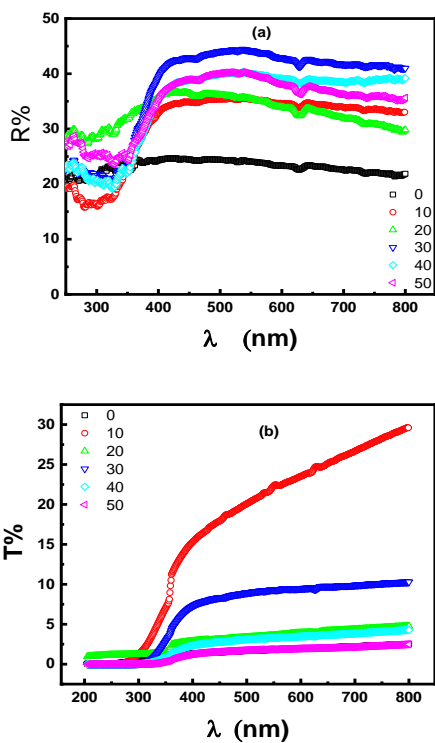

Fig.9 Spectral distribution of **a** reflectance (R) and **b** transmittance (T) for xPbO-(50-x)ZnO-50P$_2$O$_5$ where PbO = 0,10,20,30,40 and 50mol

Fig. 9(b) shows that there is no transmission for ultraviolet radiation in the U.V. region to be used as a protective glass from ultraviolet radiation. Also, the studied samples transmit visible light, which means that they are transparent glass.
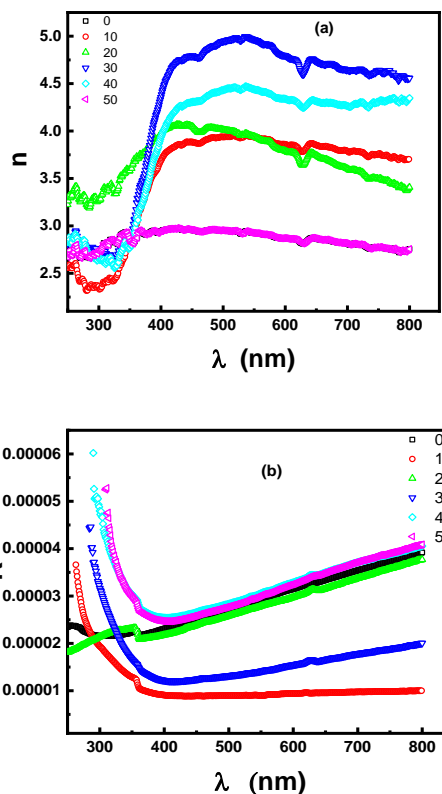

Fig. 10 Spectral dependence of **a** the refractive index (n) and **b** the extinction coefficient (k) for xPbO-(50-x)ZnO-50P$_2$O$_5$ where PbO = 0,10,20,30,40 and 50mol %

3.5.2 Spectral distribution of the "absorption coefficient α":

The "UV absorption spectra" analysis is a valuable tool for investigating the optical bandgap in amorphous systems. The interplay of "electromagnetic waves" with electrons in the valence band causes electrons to rise from the basic gap to the conduction band in optical transitions. These optical transitions might be direct or indirect, and they can be permitted or prohibited[16]. The absorption edge in many amorphous materials occurs at elevated energy scope [$\alpha > 10^4$cm^{-1}] obeys "Tauc's law" so the energy gap can be calculated as shown[25]:

$$\alpha(\nu) = \frac{B(h\nu - Eg)^r}{h\nu} \qquad [11]$$

where *B* is a constant E_g representing the optical band gap, r is an exponent, which indicates for the direct transition when r= 2 or 3, and for the indirect transition when r=1/2 and r = 3/2 allowed or forbidden, respectively. To differentiate between the various exponents and identify the transition type, we need to identify E_g magnitude. This problem may be overcome by having previous information of the absorption spectrum, which is defined as "the imaginary portion of the dielectric permittivity, ε_2, as a function of photon energy".[23]

The definite magnitude of energy gap for the studied glass samples can be established from the imaginary

part of the dielectric permittivity ε_2, $\varepsilon_2= 2nk$, when it is plotted against the energy eV. When the beginning of the "absorption spectrum (ε_2 vs. hν)" is driven, the value of the energy gap is consequently attained. Fig.11 and table 3 show the magnitude of ε_2 as a function of, E = hν, in eV for xPbO-(50-x) ZnO-$50P_2O_5$(where x=0,10,20,30,40,50) system[23]
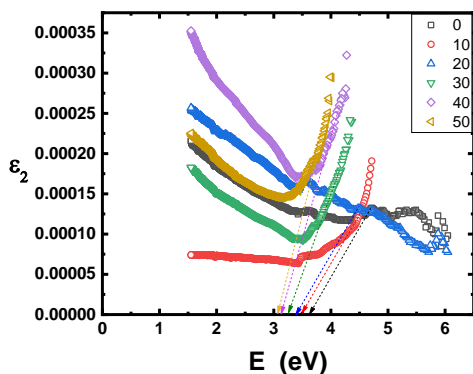
Fig.11 The imaginary part of ε_2 as a function of photon energy (hν) for xPbO-(50- x)ZnO-$50P_2O_5$ where PbO = 0,10,20,30,40 and 50mol %

As the magnitude of r is attained by using eq.11 that includes constructing a plot of "$(\alpha h\nu)^{1/r}$" vs "hν". The energy gap can be attained by prolonging the lined parts of the attained plot as revealed in Fig.12(a,b), while B can be estimated consequently from the inclined lined parts of the attained plot.
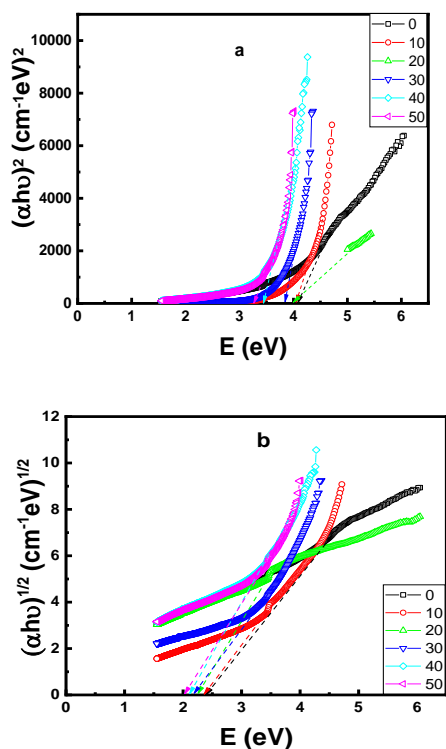

Fig. 12 Optical gaps as produced by extrapolating the linear parts of the absorption edge **(a)** E_g with r = 1/2, **(b)** E_g with r = 2 for xPbO-(50-x)ZnO-$50P_2O_5$ where PbO = 0,10,20,30,40 and 50mol %.

Fig.12(a,b) shows that the indirect and direct energy gap decrease while the ratio of lead oxide increases. Applying the results obtained from the absorption band (ε_2 vs. E of Fig.11) and table 3, it is noted that the values of the optical band gap of ε_2 is near to the values of the optical band gap of $E_g(r = 1/2)$ and thus the transition is indirect allowed one. The result for the investigated samples is in close alignment with the finding in [26].

The Urbach energy, also known as the band tail width (E_e), is used to measure the disorder in the amorphous system.[16] The Urbach energy (E_e) values were calculated from Fig.13 by taking the reciprocal of the gradients of lined parts of the plots revealed in table3. where Urbach rule for amorphous constituents is specified by[11],

$\alpha(\nu)=C\exp(h\nu/E_e)$ [12]

where *C* is constant, and E_e is the Urbach energy. The results which are given in table 3, show that the Urbach energy increases with the increased ratio of PbO, other than the energy gap. Also, the results of Urbach energy are compatible with ref.[26]

Fig. 14 shows the variation of energy gap E_g (r = 1/2) and the band tail width E_e with the PbO concentration.
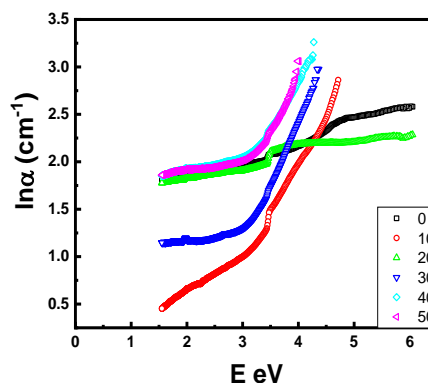

Fig. 13: Plots of ln α as a function of photon energy (hν) for xPbO-(50- x)ZnO-$50P_2O_5$ where PbO = 0,10,20,30,40 and 50mol %.

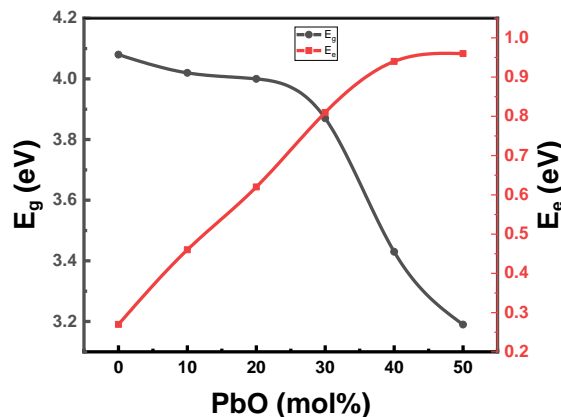**Fig. 14:** PbO concentration-dependent variations of direct optical bandgap energy for xPbO-(50- x)ZnO-$50P_2O_5$ where PbO = 0,10,20,30,40 and 50mol %

Table3: Optical parameters as estimated, E_g is the optical gap, E_e is band tail width, and $E_g (\varepsilon_2)$ is the energy calculated from the imaginary part of the dielectric constant.

Sample	E_g (r = 1/2) (eV) (indirect)	E_e (eV)	$E_g (\varepsilon_2)$
0PbO	4.08	0.27	3.65
10PbO	4.02	0.46	3.5
20PbO	4	0.61	3.42
30PbO	3.87	0.8	3.29
40PbO	3.43	0.93	3.12
50PbO	3.19	0.95	3.09

Furthermore, the optical conductivity of the glass samples has been estimated by;

$$\sigma = \alpha n c / 4\pi \qquad [12]$$

in which α is the "absorption coefficient", n is the "refractive index", and c is the "speed of light". Fig.15 displays the relationship among the "optical conductivity" and the "photon energy" for the constructed glasses, which shows that the optical conductivity increases as the ratio of PbO increases.
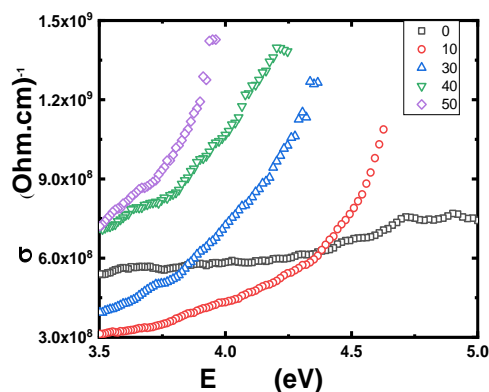

Fig. 15: Optical conductivity for xPbO-(50- x)ZnO-50P$_2$O$_5$ where x= 0,10,20,30,40 and 50mol %.

The rise in the value of NBOs due to the formation of new coordination states can be ascribed to the drop in optical band gap with the rising incorporation of PbO to binary ZnO–P$_2$O$_5$ glasses. ZnO has been shown to interact in the glass matrix in two distinct coordinating forms: octahedral and tetrahedral. By disrupting the oxygen bonds, the incorporation of PbO causes the glassy matrix chain to expand, forming a new coordinate of PbO structural units in the glass system. This might explain why the absorption edge changes into lower energy, resulting in a reduction in the optical gap and, as a result, an improvement in Urbach energy for this glass system. According to the initial hypotheses, when the content of Pb^{2+} ions rises, lesser bridged oxygens are maintained, and non-

bridged oxygens in the glass structure rise, resulting in a drop in optical band gap energies and an elevation e in the Urbach energy for the glass system. Furthermore, the optical energy gap values significantly impact the total magnitude of the "optical dielectric constant" and "optical conductivity"[26].

3.3.6 Gamma attenuation

^{137}Cs(662 keV) and ^{60}Co(1173 and 1332 keV) gamma sources were used to study the capability of attenuation of γ-photon in the investigated glass samples.

The assessed levels of γ-rays conveyed via glassy boundaries were assumed as a function of boundaries widths. The "linear attenuation coefficient μ" is obtained as the slope of attenuation curves. The values of linear attenuation coefficients were constructed against PbO percentage in the glass system, as shown in fig.16. It is observed from the figure that the "linear attenuation coefficients" of all glass systems increased directly with elevated PbO content by about half the upper limit of PbO% in the examined specimens. And it was found that the glass sample with highest PbO concentration (50 mol%) is the best to use as a shielding glass since it has higher linear attenuation coefficient especially at 1173 KeV.
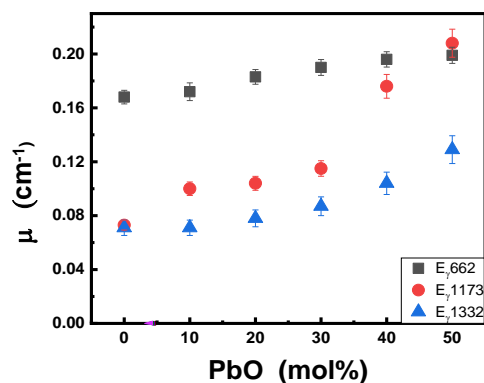

Fig. 16: Linear attenuation coefficient of the investigated glassy as a function of PbO concentration at different gamma ray energies.

The theoretically and experimentally findings of "mass attenuation coefficients" in energy dependency "$\sigma_{exp.}$& σ_{theo}" for diverse PbO content were displayed in fig.17. As the energy of gamma rays rises, there is a small reduction in "mass attenuation coefficients," this may be credited to the "Compton scattering interaction" in this intermediate energy region. Additionally, fig.17. shows an excellent match among investigational "mass attenuation coefficients" and computed predicted results by "WinXcom program (version 3.1)" [27].
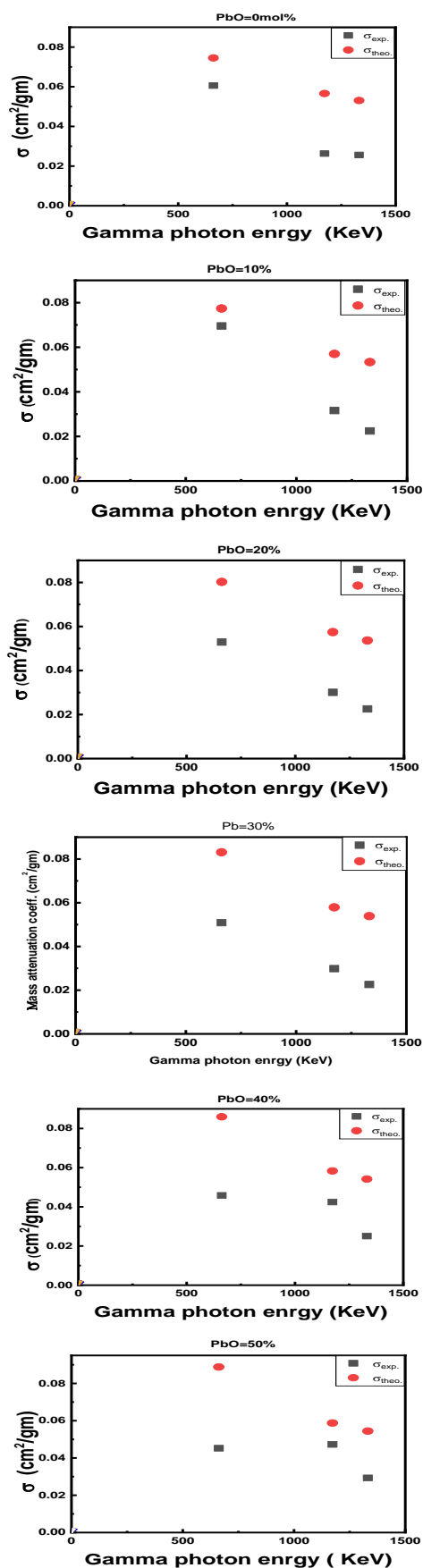
Fig. 17: Experimental and theoretical mass attenuation coefficients of glass samples as a function of gamma ray energies
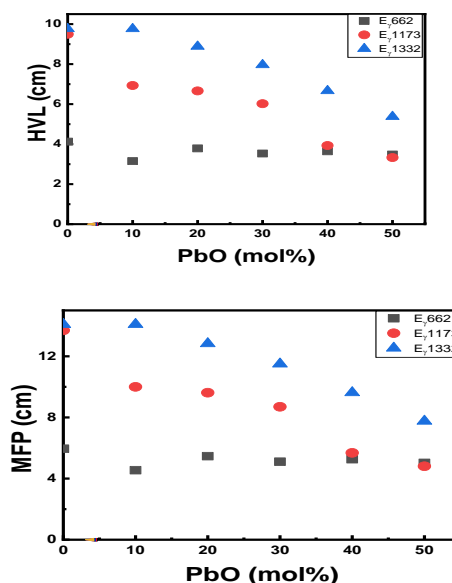

Fig. 18: (a) Half value layer of the investigated glass samples as a function of PbO concentration at different gamma ray energies, **(b)** Mean free path of the investigated glass samples as a function of PbO concentration at different gamma ray energies.

The half value layer "HVL" and mean free path "mfp" for the glass barrier samples were calculated and tabulated in table4(a&b) for diverse PbO content. The table indicated that raising the Pb ratio from 0% to 50% resulted in a decrease in "HVL" and "mfp" ranging from 6.90% to 60.92% and 15.57% to 64.90% for all energy lines, respectively

As shown in table4(a,b) and fig.18(a,b), the values of the "HVL" and the "mfp" are inversely proportional to the lead concentration where they decrease with the increasing ratio of Lead except $E\gamma 662$ there is a slight decrease because it is a monoenergetic gamma-rays [28].

The results obtained from figures (16,17&18) and table 4(a&b) may be due to the higher atomic number and density of PbO as compared to ZnO. So, (50 P2O5 – 50 PbO) glass sample is suggested as an excellent attenuator and may be utilized as a shielding glass material because, it has the higher linear attenuation, the lower mean free path and lower half value layer.[14]

4.4 Conclusion:

In this work the gamma radiation shielding parameters, structural and optical properties of $xPbO-(50-x)ZnO-50(P_2O_5)$ glass system, where x = 0,10,20,30,40,50 mol% were carried out along with density and hardness. The obtained FTIR spectra indicate that all bands shifted to lower wavenumber as PbO ratio increases from G0 to G50 except the band which is linked to the NBOs atoms P-O⁻, lifted to advanced wave number, and it is comparative to the content of ZnO is substituted by PbO, which indicates that the NBOs upsurge.

Table4:a) The values of Half Value Layer for the samples at all concentrations Pb and at the different γ -ray sources

γ -ray energy (keV)	0PbO mol%	10PbO mol%	20PbO mol%	30PbO mol%	40PbO mol%	50PbO mol%	$(HVL_{0\%}-HVL_{50\%})/HVL_{0\%}*100$
662	4.12	3.15	3.786	3.35	3.64	3.48	6.9
1173	9.49	6.93	6.66	6.02	3.93	3.33	64.92
1332	9.76	9.76	8.88	7.96	6.66	5.37	44.97

Table4 :b) The values of Mean Free Path for the samples at all concentrations of Pb and the different γ -ray sources

γ- ray energy (keV)	0PbO mol%	10PbO mol%	20PbO mol%	30PbO mol%	40PbO mol%	50PbO mol%	$(MFP_{0\%}-MFP_{50\%})/MFP_{0\%}*100$
662	5.95	4.54	5.46	5.10	5.26	5.02	15.57
1173	13.69	10.00	9.61	8.69	5.68	4.80	64.90
1332	14.08	14.08	12.82	11.49	9.61	7.75	44.96

It is also observed that the relative intensity and the relative area decrease with the increase of PbO amount except the bands which belong to P=O since it increases with the increased ratio of Pb. Besides, the results of density, molar volume, and hardness show an increase with the increased ratio of Pb. Furthermore, the dielectric permittivity has been calculated to determine the exact value of the optical band gap then the type of transition in the specimen, which has been a direct allowed one. The banded tail E_e was estimated, and outcomes ranged from "0.27-0.954 eV". The optical conductivity shows an increasing trend since the lead ratio increases. Finally, by raising PbO content by 50%, the findings of gamma radiation shielding parameters for this glass system improved "mass attenuation coefficient," "mfp," and "HVL," which were in perfect accordance with numerical simulations using "WinXcom software". It is concluded that the investigated phosphate glass is a transparent glass that can be used as a gamma radiation shielding glass for windows. Also, the glass samples showed zero transmission in the UV region that can be used as UV protection sunglasses.

The results showed that the highest concentration of the PbO specimen is the best one for gamma shielding applications.

References

[1] Sayyed, M. I., Zaid, M. H. M., Effendy, N., Matori, K. A., Lacomme, E., Mahmoud, K. A., & AlShammari, M. M. (2020). The influence of PbO and Bi_2O_3 on the radiation shielding and elastic features for different glasses. *Journal of Materials Research and Technology*, *9*(4), 8429-8438.

[2] Matori, K. A., Sayyed, M. I., Sidek, H. A. A., Zaid, M. H. M., & Singh, V. P. (2017). Comprehensive study on physical, elastic and shielding properties of lead zinc phosphate glasses. *Journal of Non-Crystalline Solids*, *457*, 97-103.

[3] Kaur, P., Singh, K. J., Thakur, S., Singh, P., & Bajwa, B. S. (2019). Investigation of bismuth borate glass system modified with barium for structural and gamma-ray shielding properties. *Spectrochimica Acta Part A: Molecular and Biomolecular Spectroscopy*, *206*, 367-377.

[4] Stoch, P., Stoch, A., Ciecinska, M., Krakowiak, I., & Sitarz, M. (2016). Structure of phosphate and iron-phosphate glasses by DFT calculations and FTIR/Raman spectroscopy. *Journal of Non-Crystalline Solids*, *450*, 48-60.

[5] ElBatal, H. A., Abdelghany, A. M., ElBatal, F. H., ElBadry, K. M., & Moustaffa, F. A. (2011). UV–visible and infrared absorption spectra of gamma irradiated CuO-doped lithium phosphate, lead phosphate and zinc phosphate glasses: a comparative study. *Physica B: Condensed Matter*, *406*(19), 3694-3703.

[6] Saddeek, Y. B., Kaid, M. A., & Ebeid, M. R. (2014). FTIR and physical features of Al_2O_3–La_2O_3–P_2O_5–PbO glasses. *Journal of non-crystalline solids*, *387*, 30-35.

[7] Sidek, H. A. A., El-Mallawany, R., Matori, K. A., & Halimah, M. K. (2016). Effect of PbO on the elastic behavior of ZnO–P_2O_5 glass systems. *Results in Physics*, *6*, 449-455.

[8] El-Denglawey, A., Saddeek, Y. B., El-Bahnasawy, H. H., Aly, K., Dahshan, A., Amer, T. Z., ... & Shaaban, K. S. (2020). Mössbauer and differential thermal analysis studies of iron alkali lead-phosphate glasses. *Physica Scripta*, *96*(2), 025706.

[9] Mitra, S., & Jana, S. (2015). Intense orange emission in Pr^{3+} doped lead phosphate glass. *Journal of Physics and Chemistry of Solids*, *85*, 245-253.

[10] Nabhan, E., Nabhan, A., & Abd El Aal, N. (2016). Mechanical and Structural Properties of Zinc–Sodium-Phosphate Glasses Doped with Cu2O. *American Journal of Physics and Applications*, *4*(6), 145-151.

[11] Nurul Ain, A. M., Sahar, M. R., Sazali, E. S., Azman, K., & Yahya, N. (2017). Study on optical absorption and structural bonding of lithium zinc phosphate glasses. In *Solid State Phenomena* (Vol. 268, pp. 54-61). Trans Tech Publications Ltd.

[12] Lamarsh, J. R., & Baratta, A. J. (2001). *Introduction to nuclear engineering* (Vol. 3, p. 783). Upper Saddle River, NJ: Prentice hall.

[13] Kumar, A., Singh, S. P., Elmahroug, Y., Kara, U., Tekin, H. O., & Sayyed, M. I. (2018). Gamma ray shielding studies on 26.66 B_2O_3–16GeO_2–4Bi_2O_3–(53.33–x) PbO–xPbF_2 glass system using MCNPX, Geant4 and XCOM. *Materials Research Express*, *5*(9), 095203.

[14] El-Kameesy, S. U., Youssef, G. M., El-Zaiat, S. Y., Saudi, H. A., & Abd El-Kawy, F. S. (2018). Gamma rays attenuation properties and the associated optical and mechanical behavior of development (70-x) B_2O_3-10Al_2O_3-10Na_2O-10ZnO-x PbO glasses. *Silicon*, *10*(5), 1881-1886.

[15] Chanthima, N., & Kaewkhao, J. (2013). Investigation on radiation shielding parameters of bismuth borosilicate glass from 1 keV to 100 GeV. *Annals of Nuclear energy*, *55*, 23-28.

[16] Ahmadi, F., Hussin, R., & Ghoshal, S. K. (2017). Structural and physical properties of Sm^{3+} doped magnesium zinc sulfophosphate glass. *Bulletin of Materials Science*, *40*(6), 1097-1104.

[17] Mansour, E., & El-Damrawi, G. (2010). Electrical properties and FTIR spectra of ZnO–PbO–P_2O_5 glasses. *Physica B: Condensed Matter*, *405*(8), 2137-2143.

[18] Ouis, M. A., Azooz, M. A., & ElBatal, H. A. (2018). Optical and infrared spectral investigations of cadmium zinc phosphate glasses doped with WO_3 or MoO_3 before and after subjecting to gamma irradiation. *Journal of Non-Crystalline Solids*, *494*, 31-39.

[19] Saddeek, Y. B. (2011). Network structure of molybdenum lead phosphate glasses: Infrared spectra and constants of elasticity. *Physica B: Condensed Matter*, *406*(3), 562-566.

[20] Abid, M., Belfaquir, M., Hafid, M., & Taibi, M. (2019). Study of zinc and lead addition effect on structure-properties of phosphate glasses. *Materials Today: Proceedings*, *13*, 458-465.

[21] Shih, P. Y. (2003). Properties and FTIR spectra of lead phosphate glasses for nuclear waste immobilization. *Materials chemistry and physics*, *80*(1), 299-304.

[22] Liu, H. S., Chin, T. S., & Yung, S. W. (1997). FTIR and XPS studies of low-melting PbO-ZnO-P_2O_5 glasses. *Materials chemistry and physics*, *50*(1), 1-10.

[23] Mady, H. A., Negm, S. E., Moghny, A. A., Abd-Rabo, A. S., & Bahgat, A. A. (2012). Study of optical properties of highly oriented nanocrystalline V_2O_5· nH_2O films doped with K ions. *Journal of sol-gel science and technology*, *62*(1), 18-23.

[24] Abdel-Gayed, M. S., Elbashar, Y. H., Barakat, M. H., & Shehata, M. R. (2017). Optical spectroscopic investigations on silver doped sodium phosphate glass. *Optical and Quantum Electronics*, *49*(9), 1-12.

[25] Madhuri, K. V., Naidu, B. S., Hussain, O. M., Eddrief, M., & Julien, C. (2001). Physical investigations on electron beam evaporated V_2O_5–MoO_3 thin films. *Materials Science and Engineering: B*, *86*(2), 165-171.

[26] Marzouk, M. A., ElBatal, F. H., & ElBatal, H. A. (2018). Investigation of ZnO-P_2O_5 glasses containing variable Bi_2O_3 contents through combined optical, structural, crystallization analysis and interactions with Gamma Rays. *Silicon*, *10*(2), 615-625.

[27] Saeed, A. (2014). RM el shazly, YH elbashar, AM Abou el-azm, MM el-Okr, MNH Comsan, AM Osman, AM Abdal-monem, AR el-Sersy, "gamma Ray Attenuation in Developed Borate glassy". *Radiaion. Physics Chemistry*, *102*, 167-170.

[28] Chang, D. S., Lasley, F. D., Das, I. J., Mendonca, M. S., & Dynlacht, J. R. (2014). Characteristics of photon beams. In *Basic Radiotherapy Physics and Biology* (pp. 69-76). Springer, Cham.